Received: 26 February 2021 | Revised: 18 February 2022 | Accepted: 27 March 2022

IET Image Processing

DOI: 10.1049/ipr2.12513

The Institution of Engineering and Technology WILEY

ORIGINAL RESEARCH

Low-light image haze removal with light segmentation and nonlinear image depth estimation

Jianwei Lv[1,2] | Feng Qian[1] | Bao Zhang[1]

[1]Changchun Institute of Optics, Fine Mechanics and Physics, Chinese Academy of Sciences, Changchun, China

[2]University of Chinese Academy of Sciences, Beijing, China

Correspondence
Bao Zhang, Changchun Institute of Optics, Fine Mechanics and Physics, Chinese Academy of Sciences, Changchun 130033, China.
Email: zhangb@ciomp.ac.cn

Funding information
National Natural Science Foundation of China, Grant/Award Number: 61705225

Abstract

Hazy image obtained in the low-light environment has the characteristics of low contrast, non-uniform illumination, color cast and much noise. In this paper, a method is put forward which can be properly applied to recover low-light hazy images. The original image is first decomposed into glow layer and haze layer with a modified color channel transformation for glow artifacts and color balanced. A new light segmentation function is proposed next by using gamma correction of channel difference and setting threshold levels to determine if the pixel belongs to light source regions. Then the ambient illuminance map is estimated using maximum reflectance prior to computing the atmosphere light in the light and non-light regions. Finally, a novel nonlinear image depth estimation model is established to build the relationship between the image depth map and three image features including luminance, saturation and gradient map for the light areas. The experimental results prove that the dehazing algorithm is reliable for removing haze and glow artifacts of active light sources, reducing much noise and improving the visibility.

1 | INTRODUCTION

When taken in hazy weather, photos or videos engender degeneracy phenomenon such as color cast, poor visibility, low degree of saturation, low contrast, and so on. The haze in a real environment is generated by small surrounding air particles and small drops of water which scatters the light entering the camera. For some applications such as computer vision systems, video monitoring systems, and aerial systems, the performance of vision algorithms is severely influenced under hazy weather. The purpose of image dehazing is to eliminate haze effects as much as possible, which can improve the efficiency of computer vision-based systems.

According to Narasimhan and Nayar's theory [1], The daytime haze model supposes that the scattered atmosphere light captured by cameras contains both the direct transmission and airlight [1]:

$$I(x) = J(x)t(x) + A(1 - t(x)), \tag{1}$$

$$t(x) = e^{-\beta d(x)}, \tag{2}$$

where $I(x)$ is the observed image at a pixel x, $J(x)$ is the scene reflection or the restored image, A is the atmosphere light which is globally constant for daytime dehazing, $t(x)$ is the transmission of the scene before reaching the camera, β is an attenuation coefficient scattered by particles, $d(x)$ is called scene depth, $J(x)t(x)$ is direct transmission, and $A(1 - t(x))$ is airlight.

Based on the principle of daytime haze formation [1], many methods in daytime image dehazing have been developed to solve the ill-posed issues [2–11]. The key of their methods is to rely on kinds of image priors. Although most existing image methods are successful for daytime dehazing, they are not so effective for low-light dehazing due to the multiple active scattering light and low level of illumination. Different from using the uniformly distributed daytime sunlight as the global constant atmosphere light, an obvious glow effect can be produced by active lights in low-light hazy images and the atmosphere light cannot be identified as the global uniform. What is more, the illumination is extremely weak and the active light glow can cover image details which is not taken into account in the common daytime dehazing research methods such as the dark channel prior(DCP) [4] and the color attenuation prior (CAP) [10]. In recent years, many novel methods are proposed such as color transfer [12], maximum reflectance prior [13], glow decomposition [15], bright alpha blending [18], image multi-scale fusion [19, 20], simultaneously dehazing and enhancement [25]. However, color shift and light glow still exist and they are not solved well after removing haze. In addition, the visibility is reduced and details of images are not so clear due to the low light environment. Low-light image enhancement methods have developed and obtained effective results [21–24], but dehazing and enhancing are two independent issues in their research. As a result, ambient illumination is dim and haze remains in low-light restored images. Although the method proposed by [25] combines dehazing process with enhancement properly, some haze still exists in their dehazing results. According to the above description, we find that the current mainstream low-light image dehazing methods estimate the atmosphere light and transmission from a global perspective, and do not consider the difference of atmosphere light and transmission between light source regions and non-light source regions, which will lead to insufficient estimation accuracy. Therefore, it is necessary to split the image into light source regions and non-light source regions so that we can, respectively, estimate the atmosphere light and transmission. The global atmosphere illumination is not uniform due to the existence of multiple active lights. Most of dehazing methods use dark channel prior to handle the transmission which results in insufficient estimation accuracy of transmission. In order to find a more precise estimation of transmission, we propose a nonlinear image depth model with three features for the light source regions.

The contributions in this paper are as follows: A novel RGB color channel transform algorithm is introduced, which can recover color-balanced images. Based on the characteristics of global atmospheric illumination which is not uniform due to the existence of multiple active lights, to make the atmosphere light and transmission estimation accurate, we propose a new light segmentation method by setting a threshold value for the gamma correction of channel difference to judge if the pixel belongs to light source regions. To estimate the transmission, we present a novel nonlinear model among three image features of the image depth map for light source regions and use DCP to handle the non-light areas. By converging the transmission maps together using the above nonlinear model and DCP in a gamma correction of channel difference manner, the refined transmission map helps reduce color distortions, noise, and halos of the recovered image. Besides, this method can remove haze, make the details and the edges clear.

2 | RELATED WORK

Many researchers have started implementation studies on low-light image dehazing. Pei et al. [12] proposed a color space conversion technique from RGB to Lab as a pre-step for mapping colors, following the modified DCP and bilateral filtering to reduce haze. Although this technique can improve the visibility of the image, the output color looks unrealistic and has a severe color shift. This is caused by color transfer, where only the mathematical model is used to change the color, and no physical model is available. Zhang et al. [13] presented a night-time image haze model, which includes different illumination offsets, color balanced, and haze removed. The colors appear more realistic than [12], but this model does not take into consideration the glow influence, which leads to significant image glow artifacts. Zhang et al. [14] proposed maximum reflectance prior assuming a value of the maximum color channel intensity close to 1 with ambient illumination in daytime haze-free images. Li et al. [15] proposed a novel low-light atmosphere scattering model utilizing an atmosphere point spreading function to express glow effects. They use a layer separation method to decompose glow and remove haze with a dark channel prior. The results consist of fewer glow effects, but the sky region of the image has plenty of noise and compression artifacts, making the restored image unrealistic. Yang et al. [17] used the method of superpixel segmentation to estimate the atmosphere light, and combined image layer decomposition and dark channel prior to remove haze. While this technique obtains good dehazing results, it produces excessive intensity in the light source area, which can cause color distortion. Yu et al. [18] presented a Pixel-wise Alpha Blending process to estimate transmission, in which the transmission estimated from the dark and the bright channel priors are effectively fused into a transmission image guided by the luminance perception weights map. Ancuti et al. [19] evaluated the airlight on the image patches and recovered the haze-free image using a multiscale fusion approach. Lou et al. [26] established a linear relationship between the transmission map and haze-related features which can be worked out by using a learning-based approach. Kuanar et al. [32] proposed a Deglow convolution neural network to remove glow effects significantly and utilized a DeHaze network for dehazing on top of it. However, their methods fail to remove glow and reduce the noise of the sky area. Besides, part of the image appears a color shift.

Recently, deep learning methods such as machine learning, Generative Adversarial Networks and Recurrent Neural Networks in image dehazing have attracted more and more attention. Tang et al. [9] researched the characteristics of haze and put forward a random forest model to determine the best combination associated with haze. Cai et al. [30] adopted a DehazeNet architecture to improve the quality of the restored images. Ren et al. [31] presented to establish the mapping relationship between hazy and the corresponding haze-free images by multi-layer deep neural networks. Li et al. [35] recommended an end-to-end AOD-Net in view of convolutional neural networks, which can directly generate haze-free images. Zhang et al. [36] improved this end-to-end model connecting pyramid dehazing network. Despite these methods are able to restore daytime haze-free images, they do not perform so well on low-light hazy images. Besides, deep learning algorithms need enough training datasets. Nevertheless, image datasets including a large number of low-light hazy images and the appropriate actual haze-free images are almost impossible to obtain because of the non-uniform ambient illumination.

In this paper, we focus on problems such as atmosphere light and transmission estimation in low-light image dehazing. To better illustrate the characteristics of low-light hazy

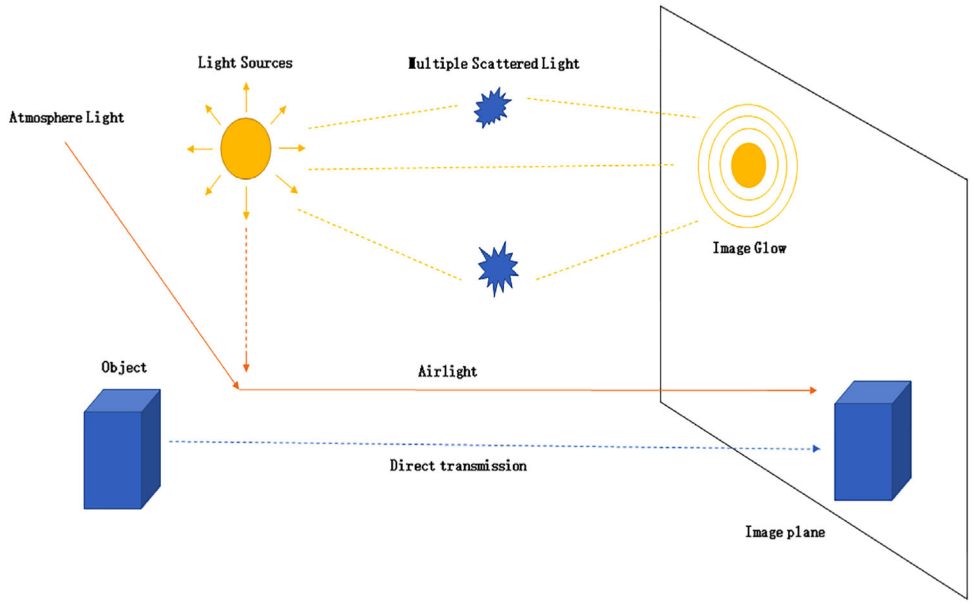

FIGURE 1 Optical imaging model for low-light haze scene and physical mechanism of APSF

images, influencing factors such as glow effect and changing illumination need to be taken into account. We propose a novel nonlinear model for transmission estimation by learning image depth-relevant features.

3 | LOW-LIGHT IMAGE DEHAZING

The presence of active light glow leads to differences in the characteristics of low-light scenes and daytime scenes. Figure 1 shows the low-light model used in our paper. According to Equation (1), the optical image model for low-light haze scenes adds an atmosphere point spread function (APSF) to a daytime model with varying atmosphere light as [15]:

$$I(x) = J(x)t(x) + A(x)(1 - t(x)) + A_L(x) * APSF, \quad (3)$$

where $A_L(x)$ is the active light sources whose intensity is convolved with APSF. $A(x)$ called atmosphere light map or ambient illuminance map which is no longer constant, and changes with different pixel position due to the contribution of light sources. This model offers a valuable way to characterize low-light hazy images with glow.

The whole process of our low-light haze removal technique is illustrated in Figure 2. The critical step is the estimation of atmosphere light map and refined transmission map. The details of the process will be described in the next sections.

3.1 | Glow decomposition

The glow is generated by the convolution of a light source with APSF expressed by the Legendre polynomial [1]. According to Equation (3), the model is simplified as:

$$I(x) = T(x) + G(x), \quad (4)$$

where $T(x) = J(x)t(x) + A(x)(1 - t(x))$ is the direct transmission and airlight, $G(x) = A_L(x) * APSF$ represents the glow of image. According to Equation (4), glow removal is considered to be an image layer decomposition issue. The ambient illumination of the glow effect is decreased smoothly, and the gradient histogram of the smooth layer has a "short tail" [16]. Therefore, the approach in [15] can be employed to decompose glow from the original image. The objective function $E(T(x))$ for glow layer separation [15] is expressed by:

$$E(T(x)) = \min \sum_x \left(\rho\left(T(x) * f_{12}\right) + \lambda\left((I(x) - T(x)) * f_3\right)^2\right.$$
$$0 \le T(x) \le I(x), \quad (5)$$

where f_{12} is the first-order filters in two directions, f_3 is the second-order Laplacian filter and the operator $*$ represents convolution. $\rho(v) = min(v^2, t)$ is a robust function which preserves large gradients of the original image $I(x)$ in the remaining haze layer $T(x)$, and the parameter t is constant which is set to 0.01. The parameter λ is important which related to the smoothness of the glow layer. When minimizing the objective function $E(T(x))$, we can get the remarkable lay separation effect.

The presence of haze usually scatters the actual light resulting in color deviation. Correcting color is a necessary step after glow decomposition. Some methods such as gamma correction, white balance correction are suitable for daytime images but cannot deal with the color shift and glows well. Zhang et al.'s maximum reflectance prior(MRP) method [14] often produces glow effects around artificial light sources. Li et al.'s color

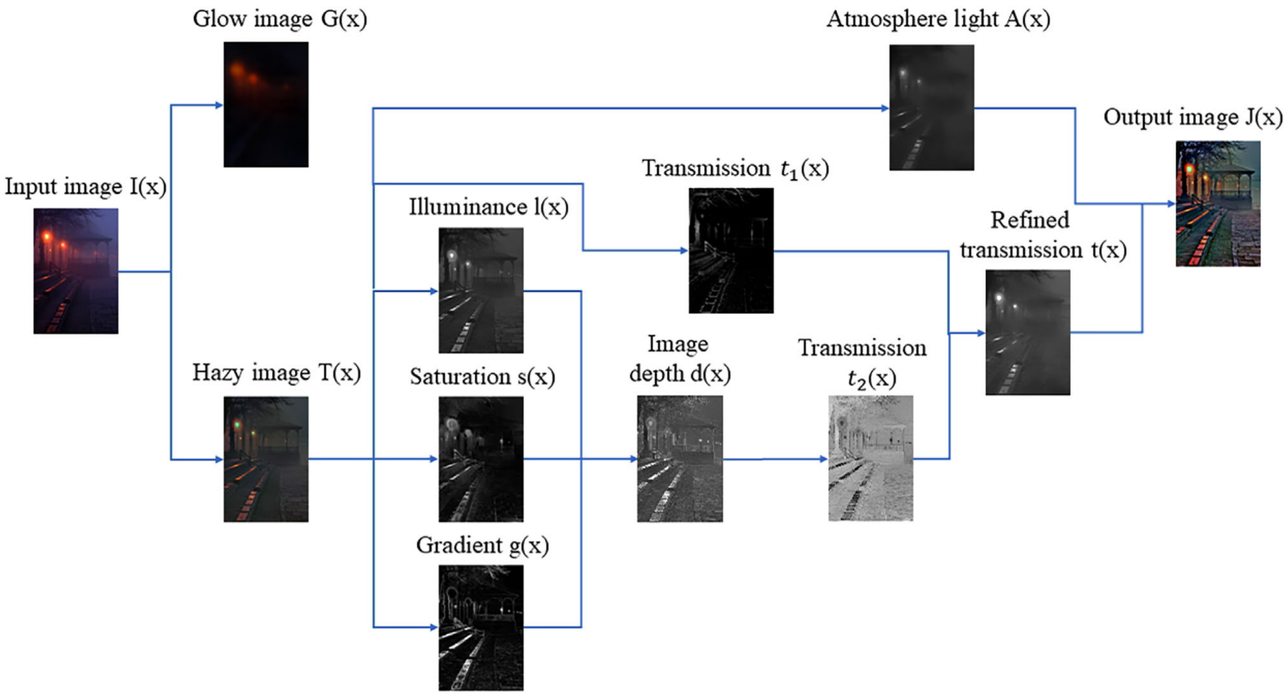

FIGURE 2 The whole process of our dehazing method

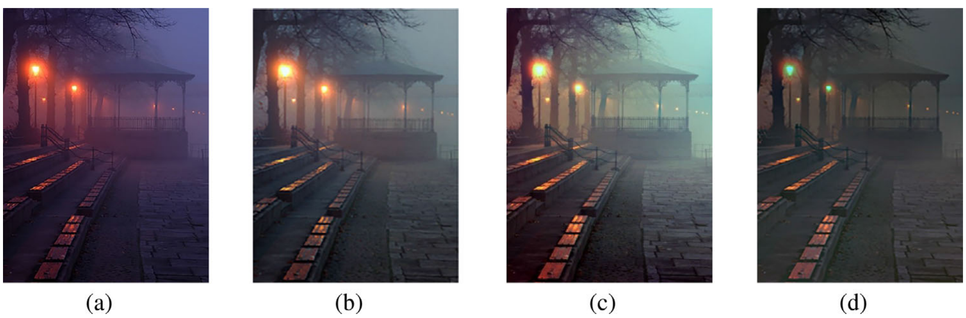

FIGURE 3 The result for color calibration. (a) Original low-light image. (b) Zhang's [14] color-corrected hazy image. (c) Li's [15] color-corrected hazy image. (d) Our result

balanced constraint method [15] still has a color-shift and halos in the edges. Therefore, a novel color transformation method is proposed to solve the color shift problem. Figure 3 shows our result after using the color channel transformation method compared with other color correction methods. Inspired by the gray world assumption method proposed in [27], the image is firstly separated into three RGB color channels. These color channels are, respectively, transformed as follows:

$$\overline{\text{Gray}} = \frac{1}{3}\left(\sum T_{\text{r}}(x) + \sum T_{\text{g}}(x) + \sum T_b(x)\right), \tag{6}$$

$$T_{r'}(x) = \frac{\overline{\text{Gray}}}{\sum T_{\text{r}}(x)} \times T_r(x), \tag{7}$$

$$T_{g'}(x) = \frac{\overline{\text{Gray}}}{\sum T_g(x)} \times T_g(x), \tag{8}$$

$$T_{b'}(x) = \frac{\overline{\text{Gray}}}{\sum T_b(x)} \times T_b(x), \tag{9}$$

where $\overline{\text{Gray}}$ is the average value of RGB channels in the image $T(x)$. r, g, and b represent the RGB space of $T(x)$, and $T_{r'}(x)$, $T_{g'}(x)$,and $T_{r'}(x)$ are the updated RGB images of $T(x)$. The obtained image is then enhanced by using single scale Retinex transform [28]. Finally, in order to smooth the edges of the image, the guided filter [29] is used for this correction.

3.2 | Light source regions segmentation

The distribution of ambient illuminance and transmission is uneven in the image because of the existence of various active light sources. This contributes to the obvious difference of ambient illuminance between light and non-light regions. So we

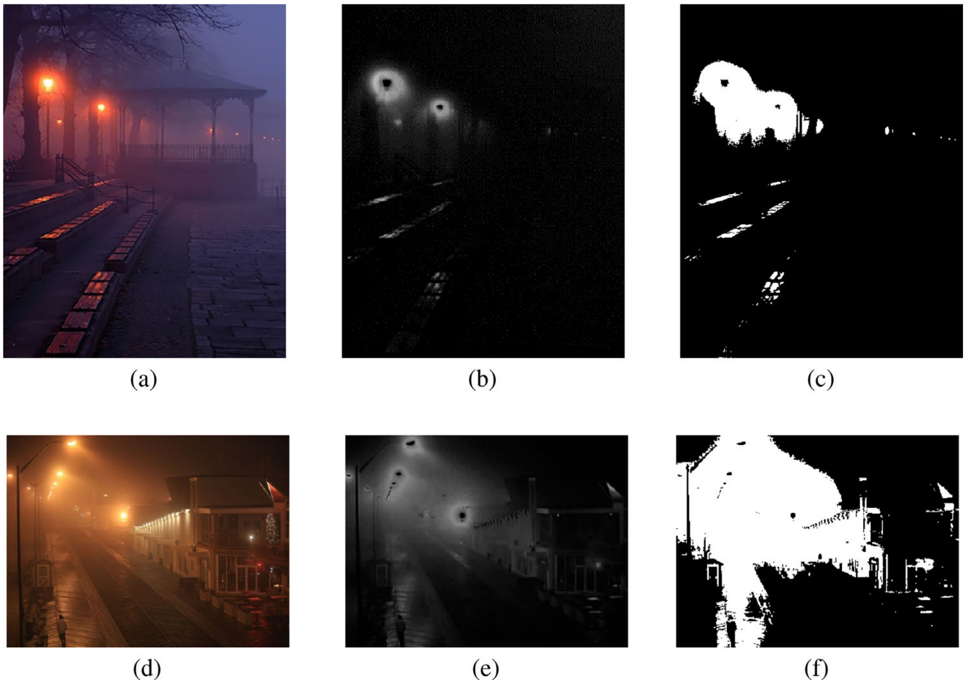

FIGURE 4 From left to right—(a) and (d): Original low-light hazy image. (b) and (e): The map of D(x). (c) and (f): Our segmentation results

need to use light source segmentation to estimate the atmosphere light and transmission, respectively, from light and non-light regions. According to the results of light segmentation, the probability of the pixel which belongs to the light source regions can be obtained. With the probability of the pixel distribution, the transmission of light and non-light regions can be combined together to obtain the global transmission.Usually in the low-light environment, there is at least one pixel with a high or low-intensity color channel value. After some experiments, we find that the channel difference between maximum intensity value and minimum intensity value in a color channel in light source regions is obviously higher than that in the non-light areas. Therefore, we can set an index called gamma correction index to enlarge this difference. In order to segment the light and non-light regions, we set a threshold to find out the boundaries of light segmentation. So mathematically, to segment the light source regions well, we can define our new function $\eta(x)$ with the gamma correction of channel difference as:

$$\eta(x) = \max_{c\in RGB}\left(I^c(x)\right) - \min_{c\in RGB}\left(I^c(x)\right)^{\gamma} = \begin{cases} \geq N^{th}, x \in LSR \\ < N^{th}, x \in NLSR \end{cases}, \tag{10}$$

where N^{th} is the threshold value which is set to segment the light source regions, LSR and NLSR represent the light source regions and the non-light source regions, respectively. In order to confirm the threshold and gamma, we select 500 night-time images with light sources and segment them, as shown in Figure 4. After experiments, we set $N^{th} = 0.07$ (the corresponding pixel value is 17.85) and $\gamma = 2.0$. The results show the higher that value of $\eta(x)$ is, the more possible the pixel is in the bright region. So we approximate the above function $\eta(x)$ as the probability that per pixel belongs to the bright areas.

3.3 | The estimation of atmosphere light map

In He et al.'s method [4], the brightest 0.1 percent of pixels in one of RGB dark channels are selected as the atmosphere light. The atmosphere light in the daytime environment is considered to be uniformly distributed, so the atmosphere light is a constant value. However, this does not apply to low-light images. There will be more noise in the sky area and the sky looks unreal in the image. What's more, low-light haze removal is not so effective. The global atmosphere light is not uniform.Therefore, just replacing the global atmosphere light estimation with a local one will make the estimation inaccurate [33]. It will influence the process of transmission estimate. To solve the above problems, an adaptive model is proposed for the atmosphere light map. In the low-light hazy image, the intensity of atmosphere light is mainly related to active light sources scattered through haze. Theoretically, the scattered intensity of multiple light sources attenuates exponentially through haze in the light areas. The airlight is produced by haze scattering the atmosphere light whose intensity increases in non-light areas. So the ambient illuminance map of the image is made up of the attenuated light in light source regions and the airlight in non-light areas. Due to the intensity of airlight in non-light source regions is so weak, we consider approximately the intensity of atmosphere light is equal to airlight. According to the above theory, we describe the

FIGURE 5 (a) The luminance map. (b) The saturation map. (c) The gradient map. (d) The image depth map

ambient illuminance map as:

$$P(x) = \begin{cases} A_0(x), x \notin LSR \\ A_1(x)t_2(x), x \in LSR \end{cases}, \tag{11}$$

where LSR is the multiple light source regions, $P(x)$ is the ambient illuminance map of the image $I(x)$, and $t_2(x)$ is the transmission in light source regions which is determined in Section 3.4. $A_0(x)$ is the atmosphere light in dark regions, and $A_1(x)$ is the atmosphere light in light regions. In order to obtain $P(x)$, MRP method [14] is used to obtain the ambient illuminance map as:

$$P(x) = \max_{c\in R,G,B} I^c(x). \tag{12}$$

After computing $t_2(x)$ in the next section, the truth atmosphere light map can be estimated by combining $A_0(x)$ and $A_1(x)$ with the probability in Equation (10) as follows:

$$A(x) = \eta(x)A_1(x) + (1 - \eta(x))A_0(x). \tag{13}$$

3.4 | The estimation of transmission map

When some existing methods such as DCP and MRP are handled separately for regions with and without light sources, the dehazing performance is not so well, we create a nonlinear model among three haze-related features for light source regions (LSR) and use DCP to handle the non-light source regions (NLSR). Having obtained the value of the atmosphere light $A_0(x)$ in non-light source regions, we can compute the transmission maps $t_1(x)$ by applying the DCP for the non-light source regions as follows:

$$t_1(x) = 1 - \min_{i\in\Omega(x)} \min_{c\in R,G,B} \left(\frac{I^c(i)}{A_0^c(i)}\right), i \in NLSR. \tag{14}$$

Theoretically, low-light hazy images have the characteristic of high brightness, low saturation, and local smoothness. Hence, we can construct a novel nonlinear model of the depth map $d(x)$ to express the haze density by the luminance $l(x)$, the saturation $s(x)$, and the gradient $g(x)$ in the light source regions, as shown in Figure 5. We propose the image depth estimation map $d(x)$ as:

$$d(x) = \frac{1}{1 + e^{-\lambda(\omega_1 l(x) + \omega_2 s(x) + \omega_3 g(x) + \varepsilon)}}, x \in LSR, \tag{15}$$

where x is the value of per pixel of the image, $\omega_1, \omega_2, \omega_3$ are the non-linear parameters, ε represents the random error of this model.

To determine the unknown coefficients, we collect numbers of low-light hazy images are collected from www.flickr.com, www.gettyimages.com, and D-HAZY dataset [20]. Synthetic depth maps and corresponding hazy images are generated to obtain sufficient training samples, as seen in Figure 6.

First, we randomly generate a haze depth map with an open interval of (0.5, 1) for each haze-free image. Secondly, We produce a vector $A(k, k, k)$ of atmosphere light, where k is a parameter between 0.80 and 1.0. Finally, we collect 1000 nighttime haze-free images and 1000 synthetic hazy images with the above image depth $d(x)$ and atmosphere light $A(k, k, k)$. Besides, we obtain the luminance maps, the saturation maps, and the gradient maps of all these nighttime hazy image samples. According to Equation (15), our training model of the haze depth map $d_\omega(x_i)$ can be simplified as follows:

$$d_\omega(x_i) = \frac{1}{1 + e^{-\lambda(\omega^T X_i + \varepsilon)}}, \tag{16}$$

where i is the number ith training sample, $\omega^T = [\omega_1, \omega_2, \omega_3]^T$ and $X_i = [l(x_i), s(x_i), g(x_i)]$, our hazy image depth map of the ith training sample is represented as $d^{(i)}$. n is the total number of training samples. Then the following cost function $E(\omega, \lambda, \varepsilon)$ is expressed as [34]:

$$E(\omega, \lambda, \varepsilon) = -\frac{1}{n} \times \left[\sum_{i=1}^{n} \left(d^{(i)} \log\left(d_\omega\left(x^{(i)}\right)\right) + \left(1 - d^{(i)}\right) \log\left(1 - d_\omega\left(x^{(i)}\right)\right)\right)\right]. \tag{17}$$

After having obtained the cost function, we initialize $\lambda = 5.0, \omega_1 = 1.0, \omega_2 = -1.0, \omega_3 = 1.0, \varepsilon = 0.1$. In addition, we assign the Learning Rate μ of 0.001. As for other non-linear

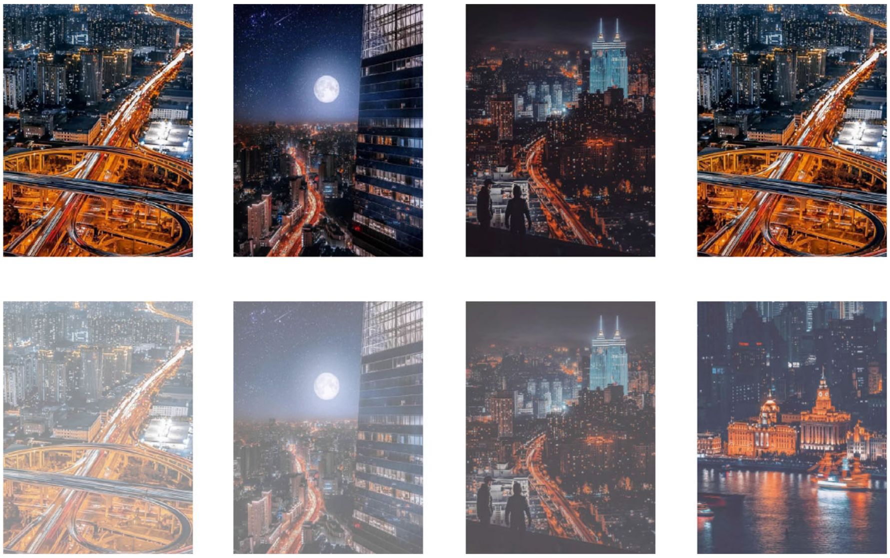

FIGURE 6 The example of low-light haze-free images and the corresponding hazy images. Top row: low-light haze-free images. Bottom row: hazy images

coefficients $\lambda, \omega_1, \omega_2, \omega_3, \varepsilon$, an adaptive stochastic gradient descent(SDG) algorithm [34] is adopted as follows:

$$\omega_i := \omega_i - \mu \frac{\partial E(\omega_1, \omega_2, \omega_3)}{\partial \omega_i}, \tag{18}$$

$$\lambda_i := \lambda_i - \mu \frac{\partial E(\lambda)}{\partial \lambda_i}, \tag{19}$$

$$\varepsilon_i := \varepsilon_i - \mu \frac{\partial E(\varepsilon)}{\partial \varepsilon_i}. \tag{20}$$

After learning and training image samples, the final results are that $\lambda = 2.5, \omega_1 = 0.8267, \omega_{12} = -0.2968, \omega_3 = 0.5245, \varepsilon = 0.041327$. If these parameters are determined, the following equation can be employed to estimate the image transmission of light source areas:

$$t_2(x) = e^{-\beta d(x)}. \tag{21}$$

Note that $t_1(x)$ and $t_2(x)$ are separately effective in non-light and light areas, it is essential to combine them together to get the global transmission $t(x)$. According to the Equations (10), (14), (15), and (21), we use the light segmentation function $\eta(x)$ as the probability to blend the transmission $t_1(x)$ and $t_2(x)$ together. The following transmission $t(x)$ is estimated as:

$$t(x) = \eta(x)t_2(x) + (1 - \eta(x))t_1(x). \tag{22}$$

(Algorithm 1)

Our transmission map is shown in Figure 7. It is worth noting that Equation (15) uses a similar model proposed in Zhu et al.'s color attenuation prior method [10], and they all contain saturation and brightness components. However, our gradient component related to the image details and training method is different from what they use, since low-light hazy images are normally low saturation, reduced contrast, unclear details, and high luminance in the light source area. The Laplacian components are used to express the gradient component because they highlight the information of edges. Although the haze feature components are the same as Lou's method [26], the proposed model is a non-linear Sigmond function, and we estimate the unknown coefficients by the adaptive SGD algorithm [34]. The non-linear Sigmond function is utilized to control the value of the depth map from 0 to 1. In addition, the non-linear model

ALGORITHM 1 Algorithm of nonlinear image depth estimation model

Input: illuminance vector $l(x)$, saturation vector $s(x)$, gradient vector $g(x)$, image depth $d(x)$ of each synthetic hazy image from the training dataset, learning Rate μ.

Output: Nonlinear parameters $\lambda, \omega_1, \omega_2, \omega_3, \varepsilon$.

```
Initialization: λ = 5.0, ω1 = 1.0, ω2 = −1.0, ω3 = 1.0, ε = 0.1.
p = 0, q = 0, r = 0, s = 0, v = 0, μ = 0.001;
for each i ∈ [1, n] do
    t = d_ω(x_i) − d^(i);
    t1 = ω1 l(x) + ω2 s(x) + ω3 g(x) + ε;
    p = p + t ∗ (1 − d^(i)) ∗ d^(i) ∗ λ;
    q = q + t ∗ (1 − d^(i)) ∗ d^(i) ∗ λ ∗ l(xi);
    r = r + t ∗ (1 − d^(i)) ∗ d^(i) ∗ λ ∗ s(xi);
    s = s + t ∗ (1 − d^(i)) ∗ d^(i) ∗ λ ∗ g(xi);
    v = v + t ∗ (1 − d^(i)) ∗ d^(i) ∗ t1;
end for
ε = ε + μ ∗ p/n;
ω1 = ω1 + μ ∗ q/n;
ω2 = ω2 + μ ∗ r/n;
ω3 = ω3 + μ ∗ s/n;
λ = λ + μ ∗ v/n;
```

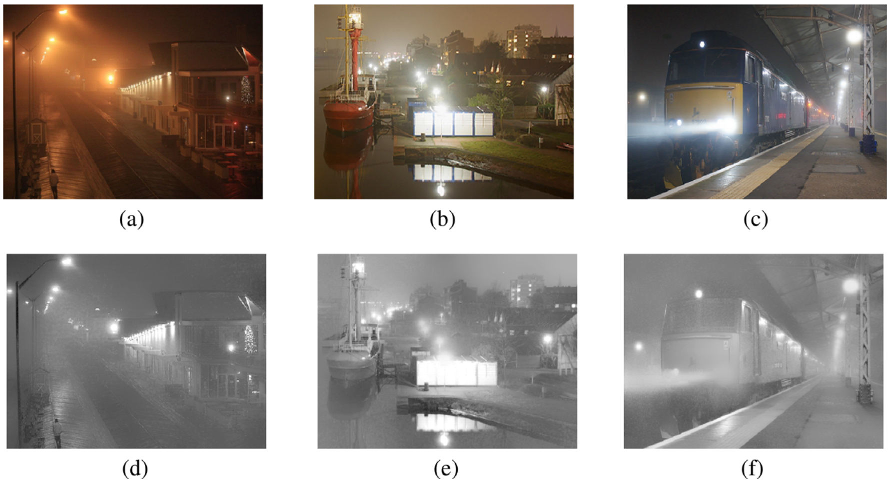

FIGURE 7 Example images and the estimated transmission maps. Top row: (a)–(c) the input hazy images. Bottom row: (d)–(f) the transmission maps

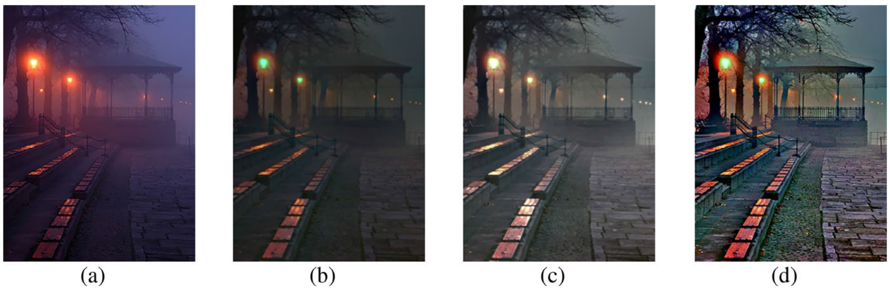

FIGURE 8 (a): Input low-light hazy image. (b)–(d): The dehazing results using $t_1(x)$, $t_2(x)$ and $t(x)$

can describe the depth map well and better improve the transmission estimation.

We apply the image guided filter to smooth and preserve the edges of the transmission map. Figure 8 shows our dehazing results using our combined transmission model. It is clear that the transmission estimated by DCP tends to deal with haze well in dark areas while the transmission estimated by our nonlinear model shows good preservation and smoothness of shapes and edges of objects in light areas.

Due to the large black area, the lower limit of transmission can not reach a very small value, so we take 0.10 as the limit which can get better recovery of the image. After Achieving the values of $t(x)$ and $A(x)$, we restore the following low-light hazy image as:

$$J(x) = \frac{I(x) - A(x)}{\max(t(x), 0.1)} + A(x). \tag{23}$$

(Algorithm 2)

4 | EXPERIMENT RESULTS

To demonstrate the effectiveness of our dehazing method, we have implemented the experimental results of the algorithm and compare our results with the widely-used dehazing methods such as dark channel prior(DCP) [4] with HDRnet [37], Zhang's new image model (NIM) [13], Zhang's maximum reflectance prior (MRP) [14] method, Cai's DehazeNet [30], Ren's multi-scale convolutional neural networks (MSCNN) [31], Lou's Haze Density Features (HDF) method [26], Li's Glow Decomposition and Multiple Light Colors (GDM) method [15], Yu's Pixel-wise Alpha Blending (PAB) method [18], respectively. The algorithms are implemented in the software MATLAB R2019a on the Inter Corei7-7500U 2.90GHz, 8GB RAM. The parameters of our learning model are obtained as follows: $\beta = 0.5, \lambda = 2.5, \gamma = 2.0, \mu = 0.001, \omega_1 = 0.8267, \omega_2 = -0.2968, \omega_3 = 0.5245, \varepsilon = 0.041327$.

4.1 | Qualitive evaluation on real-world images

As shown in all figures, DCP with HDRnet, DehazeNet, and MSCNN tend to fail to remove haze and glow artifacts in real low-light hazy images. In Figures 9b,e,f, the brightness of dehazing images appear more dark and the dehazing results present a certain image glow. It is concluded that they are suitable for daytime dehazing but they are not effective for low-light image

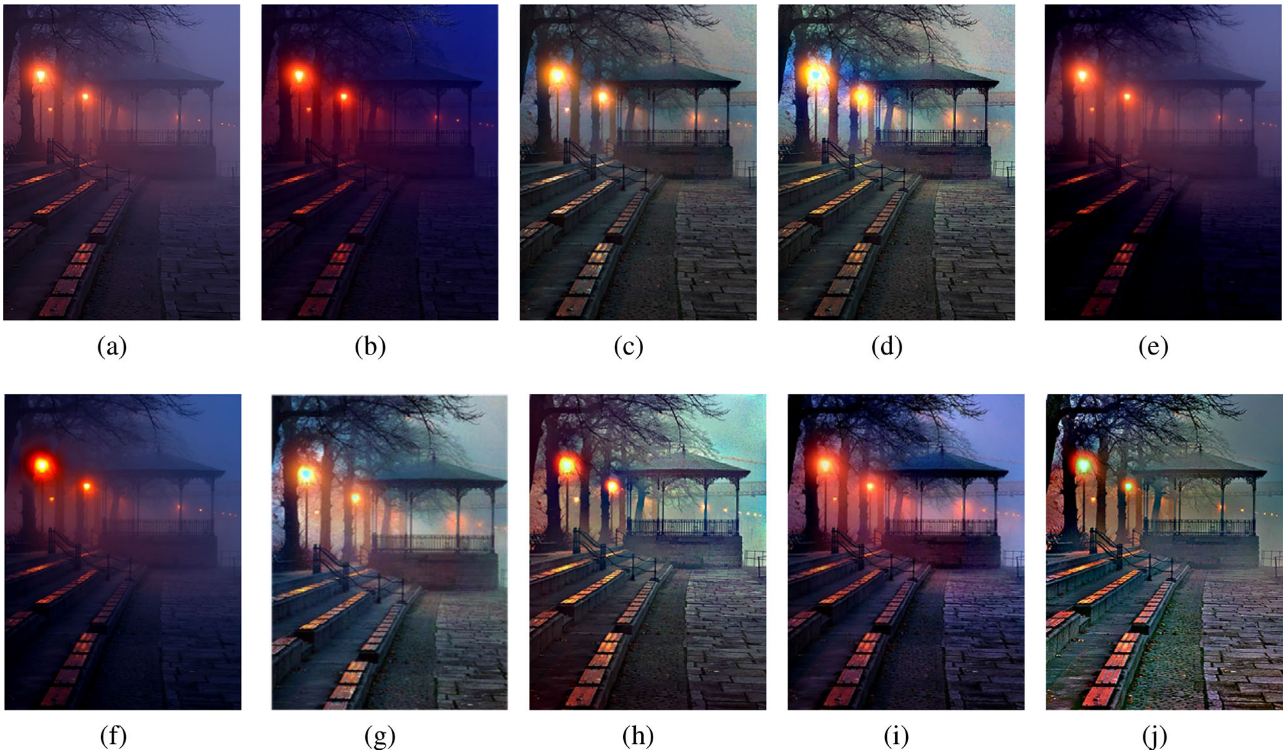

FIGURE 9 Visual comparisons of dehazing methods on real images. (a) Low-light hazy images. (b) DCP+HDRnet. (c) NIM. (d) MRP. (e) DehazeNet. (f) MSCNN. (g) HDF. (h) GDM. (i) PAB. (j) Ours

ALGORITHM 2 Algorithm of restoring a low-light hazy image

Input: low-light hazy image $I(x)$; low-light hazy image model
$I(x) = J(x)t(x) + A(x)(1 - t(x)) + A_L(x) * APSF$

Using image decomposition to obtain glow image $G(x)$ and hazy image $T(x)$

Using color channel transformation to make the color of image $T(x)$ balance

Using light segmentation method to get the probability $\eta(x)$ in Equation (10): $N^{th} = 0.07, \gamma = 2.0$.

if x in dark regions: **then**

Using dark channel prior to get the transmission $t_1(x)$ in Equation (14).

Calculate $A_0(x)$ using Equation (12)

else

Using Equation (15) to estimate the image depth $d(x)$:

$\lambda = 2.5, \omega_1 = 0.8267, \omega_2 = -0.2968, \omega_3 = 0.5245, \varepsilon = 0.041327$.

Using Eq.(16) to get the transmission of the source regions $t_2(x)$:$\beta = 0.5$.

Using Equations (11) and (12) to obtain $A_1(x)$.

end if

Using Equation (11) to get the atmosphere light $A(x)$.

Calculate the transmission $t(x)$ using Equation (22).

Refine transmission using guided filter.

Output: Get restored image $J(x)$ using Equation (23)

dehazing. In Figures 9 and 13, although NIM, MRP, HDF, and PAB methods increase the contrast of images, strong light and large glow artifacts can be clearly observed. Besides, color shift can be seen in Figures 9c,d,g. Our proposed algorithm not only improves the contrast dramatically and deals well with large image glow, but also solve color shift problem (see in dark grove areas of Figure 9). As observed in the sky region in Figures 10, 11, and 14, other methods produce more noises and cannot be capable of dealing with the sky, while ours can significantly reduce much more noise and recover the sky regions better. The sky regions of our dehazing results look more natural in Figures 9, 11, and 14. In Figures 12 and 14, we can see that it is overexposure in white light regions using MRP, HDF, GDM, and PAB, but our method can reduce image overexposure and make the details of active light sharp. In Figures 9, 13, and 14, it is observed from the comparison that both GDM and our method have significantly reduced the glow. But our method can better preserve the original shape and edges of all light sources better. Because of the improvement of atmosphere light and transmission, our algorithm tend to restore details well in the image dark areas.

4.2 | Image quality assessment

In order to avoid the deviation of the subjective visual assessment, the objective metrics are required to evaluate the haze removal results produced by different nighttime dehazing

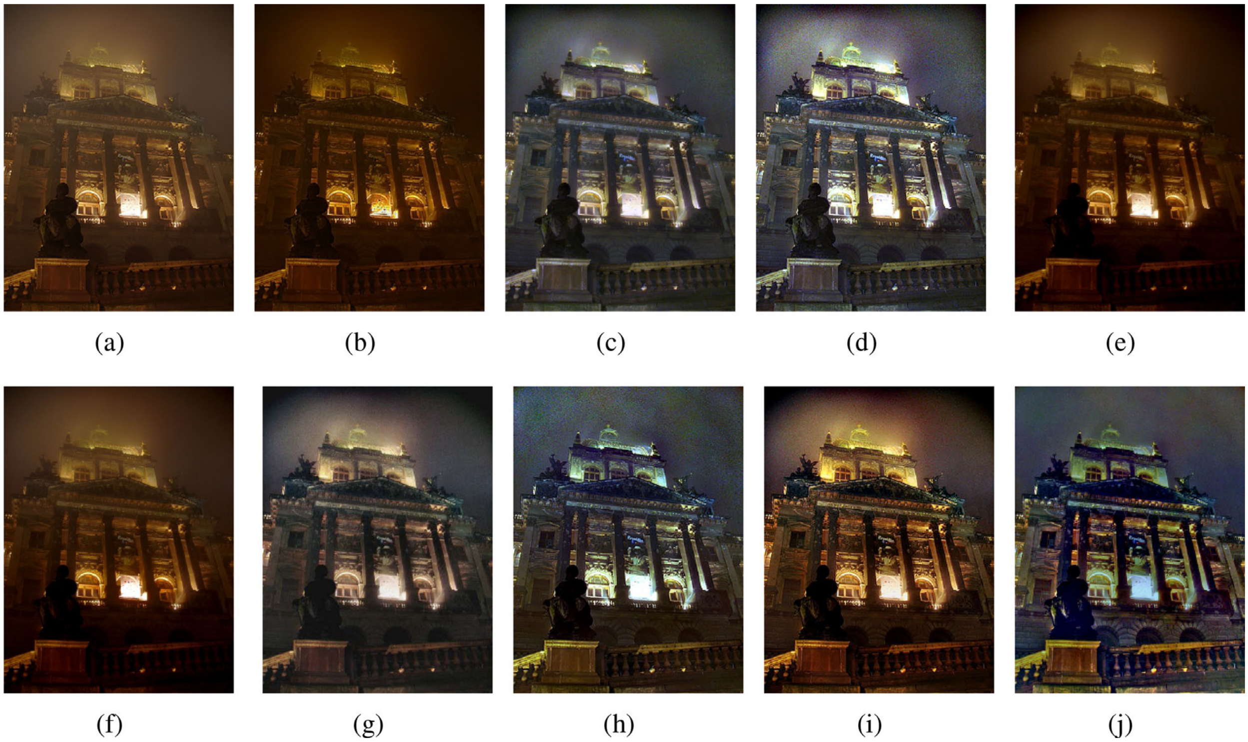

FIGURE 10 Visual comparisons of dehazing methods on real images. (a) Low-light hazy images. (b) DCP+HDRnet. (c) NIM. (d) MRP. (e) DehazeNet. (f) MSCNN. (g) HDF. (h) GDM. (i) PAB. (j) Ours

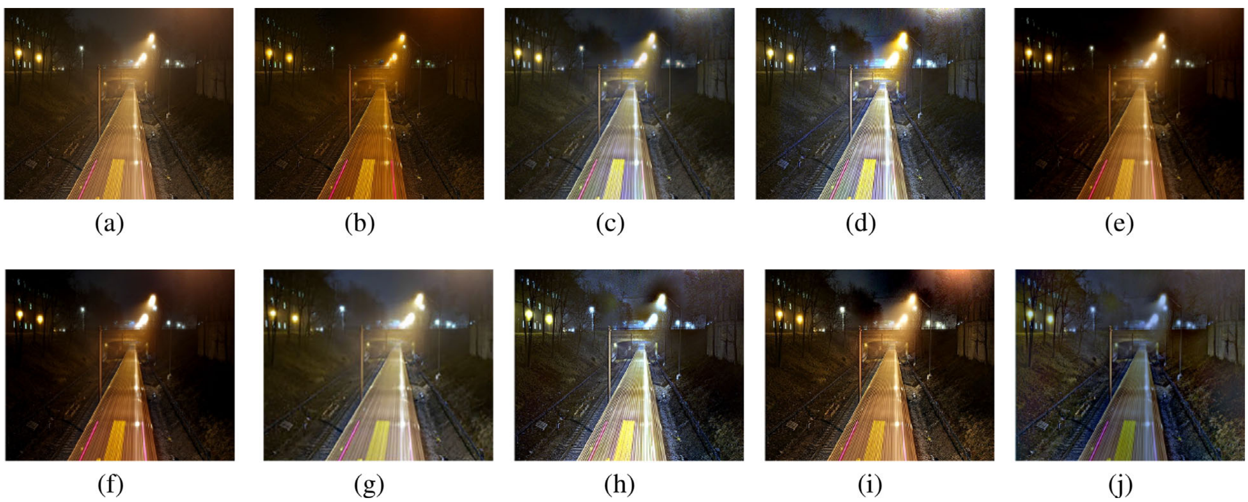

FIGURE 11 Visual comparisons of dehazing methods on real images. (a) Low-light hazy images. (b) DCP+HDRnet. (c) NIM. (d) MRP. (e) DehazeNet. (f) MSCNN. (g) HDF. (h) GDM. (i) PAB. (j) Ours

techniques. Furthermore, some well-known evaluation metrics are calculated to quantitatively assess the performance of haze removal.The image quality assessment (IQA) metrics can be divided into the non-reference metric, the reduced-reference metric, and the full-reference metric. The blind assessment [38] is a widely used non-reference metrics method which contains the parameters e and $\bar{r}$. The blind assessment e, $\bar{r}$, and image visibility measurement (IVM) [39] are used to evaluate the visible edges of the image. Larger e, $\bar{r}$, and IVM indicate that the algorithm has better edges preservation performance between the recovered image and hazy image. Blind/Referenceless Image Spatial Quality Evaluator (Brisque) [40] is another widely used no-reference IQA index. The Brisque can be used to evaluate the quality of image from many aspects. The smaller the Brisque, the better the recovered image. The peak signal-to-noise ratio (PSNR) is used to evaluate the overall quality of the algorithm. The structural similarity index (SSIM) proposed by Wang [41] is to measure the ability of structure-preserving. A higher PSNR represents the recovered result is more desirable, and a higher SSIM indicates a better spatial structure between the recovered

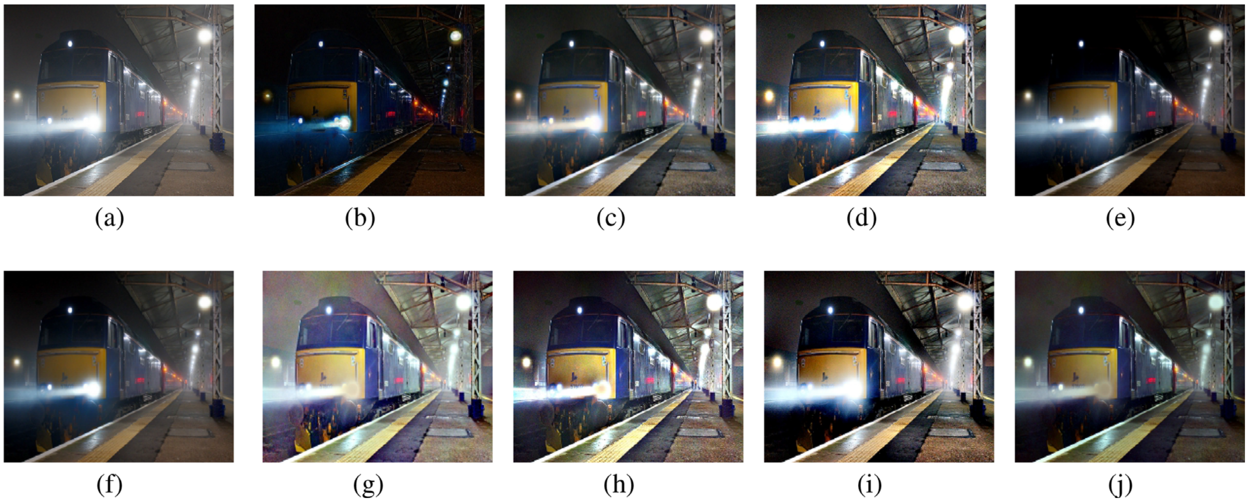

FIGURE 12 Visual comparisons of dehazing methods on real images. (a) Low-light hazy images. (b) DCP+HDRnet. (c) NIM. (d) MRP. (e) DehazeNet. (f) MSCNN. (g) HDF. (h) GDM. (i) PAB. (j) Ours

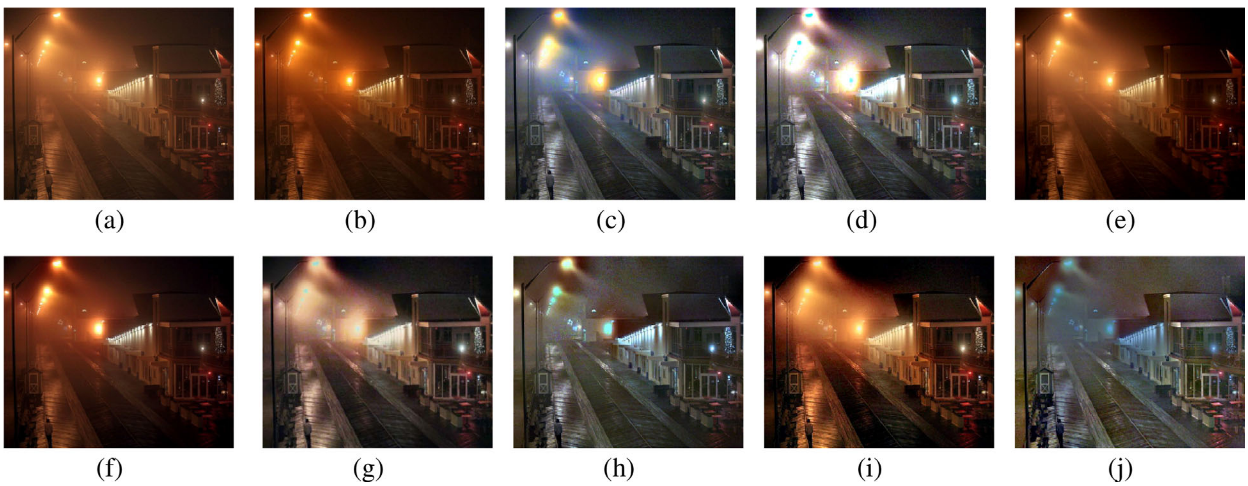

FIGURE 13 Visual comparisons of dehazing methods on real images. (a) Low-light hazy images. (b) DCP+HDRnet. (c) NIM. (d) MRP. (e) DehazeNet. (f) MSCNN. (g) HDF. (h) GDM. (i) PAB. (j) Ours

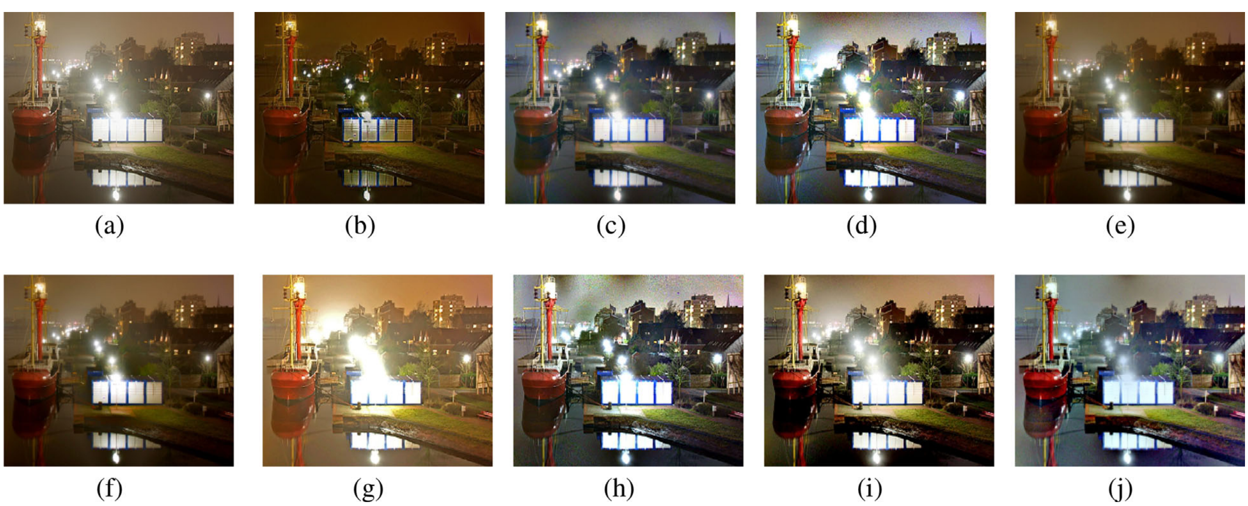

FIGURE 14 Visual comparisons of dehazing methods on real images. (a) Low-light hazy images. (b) DCP+HDRnet. (c) NIM. (d) MRP. (e) DehazeNet. (f) MSCNN. (g) HDF. (h) GDM. (i) PAB. (j) Ours

TABLE 1 The non-reference image quality assessment metrics

	Figure 9			Figure 10			Figure 11		
Metrics	e	$\bar{r}$	**Brisque**	e	$\bar{r}$	**Brisque**	e	$\bar{r}$	**Brisque**
DCP+HDRnet	10.2361	1.1671	30.1716	3.7861	1.0376	29.9362	3.9172	0.9686	47.1006
NIM	12.2767	3.0358	32.3343	19.3419	2.1186	28.5083	8.2865	1.5388	46.6019
MRP	13.7402	4.7722	29.5089	18.9168	3.5987	37.3574	9.5286	2.6240	52.7286
DehazeNet	4.8381	0.8361	32.8018	12.2459	0.9110	35.5464	9.4882	0.6450	49.0672
MSCNN	11.5766	0.9915	35.5655	8.6224	0.8316	36.1810	10.2149	0.7301	50.2617
HDF	10.9306	3.4804	31.9876	15.8912	2.1367	33.2291	10.4430	1.1105	55.9961
GDM	14.2037	4.9602	28.9453	17.9323	3.8693	41.3811	11.0834	2.5855	49.9085
PAB	13.2757	3.0975	29.9596	16.2059	3.5301	28.8763	8.3611	2.2524	49.9640
Ours	**13.8796**	**4.9217**	**28.7283**	**18.2661**	**4.2362**	**25.5843**	**14.5079**	**2.8593**	**45.3761**
	Figure 12			**Figure 13**			**Figure 14**		
Metrics	e	$\bar{r}$	**Brisque**	e	$\bar{r}$	**Brisque**	e	$\bar{r}$	**Brisque**
DCP+HDRnet	5.6822	1.1103	15.2255	8.6633	1.0796	16.6320	7.8211	1.2246	24.4154
NIM	15.3558	1.2575	25.3856	12.5735	2.2292	21.2607	8.0124	1.3335	20.7335
MRP	16.1778	2.9349	29.2990	15.6891	2.9165	16.7925	7.5419	3.1062	19.8295
DehazeNet	6.6788	0.8381	15.6019	6.0114	0.9944	15.8819	6.3343	0.8566	13.5698
MSCNN	12.5564	0.8169	14.0466	9.5873	1.0898	16.2567	6.3141	0.8715	14.8169
HDF	15.2633	2.8619	15.6008	10.9212	2.5239	19.3936	6.2900	1.7233	23.9348
GDM	17.9989	4.0069	29.0668	14.9922	2.5542	18.7978	7.1507	3.5269	24.4489
PAB	14.3456	3.1124	32.5806	15.0728	2.3674	16.7530	7.0054	2.3707	19.8185
Ours	**21.7423**	**4.5095**	**11.2453**	**15.9388**	**3.1372**	**14.4555**	**8.3600**	**3.8108**	**10.9310**

image and haze-free image. The contrast gain (CG) [42] is to measure the contrast of the image, and visual contrast measure (VCM) [43] are to quantify the degree of the image visibility. The higher the CG and VCM, the clearer the recovered image.

To quantify the dehazing results, we pick out the low-light haze-free images and the corresponding synthesized hazy images in the website www.flickr.com and Liao's paper [44] for the test. Table 1 shows the blind assessment values and Brisque of our proposed and other methods achieved by measuring the real-world images from Figures 9 to 14. As shown in Table 1, the values e and $\bar{r}$ of our method are higher than others except in Figure 9. This is because the edges of our image in Figure 9 are not clearer than GDM method. But from all the images, these indicate our method has better edges preservation performance between the recovered image and hazy image. The Brisque obtained by using our algorithm are all smaller than others. These results show that the recovered image of our method has better image quality than others. Figure 15 shows the comparison results using hazy image and the corresponding ground truth image, and Table 2 displays the IQA values of all the dehazing algorithms. It is shown that our values of e, IVM, CG, and VCM are higher than other methods. These denote that our method has better edges preservation and a larger degree of visibility improvement. Our proposed algorithm achieves the highest PSNR value, because our image depth model can better deal with the light regions. Besides, our SSIM value is the highest. This shows that our recovered image has a better spatial structure and our light segmentation method can significantly refine the atmosphere light map and the transmission map.In words, our proposed method is highly effective for low-light image haze removal.

TABLE 2 Image quality assessment using different dehazing methods

Quality assessment	e	**IVM**	**SSIM**	**CG**	**VCM**	**PSNR**
DCP+HDRnet	25.7954	8.7810	0.3202	0.2994	16.8333	15.2770
NIM	26.7448	8.0512	0.5239	0.3854	43.6667	17.5994
MRP	16.7590	8.5947	0.7671	0.3945	20.5000	21.8694
DehazeNet	25.7821	8.8623	0.3200	0.1797	15.5000	18.9668
MSCNN	11.2882	6.6786	0.4950	0.1853	18.1667	17.8850
HDF	30.5368	8.4593	0.7558	0.3572	52.6667	17.9537
GDM	32.1134	8.8646	0.7288	0.3991	25.6667	20.2104
PAB	23.2590	7.2399	0.7603	0.3159	56.0000	20.5560
Ours	**34.9572**	**9.2090**	**0.7834**	**0.4083**	**58.5000**	**21.9688**

4.3 | The execution time of our algorithm

The execution time is another key index for our dehazing method. Since it is difficult to analyze the time complexity,

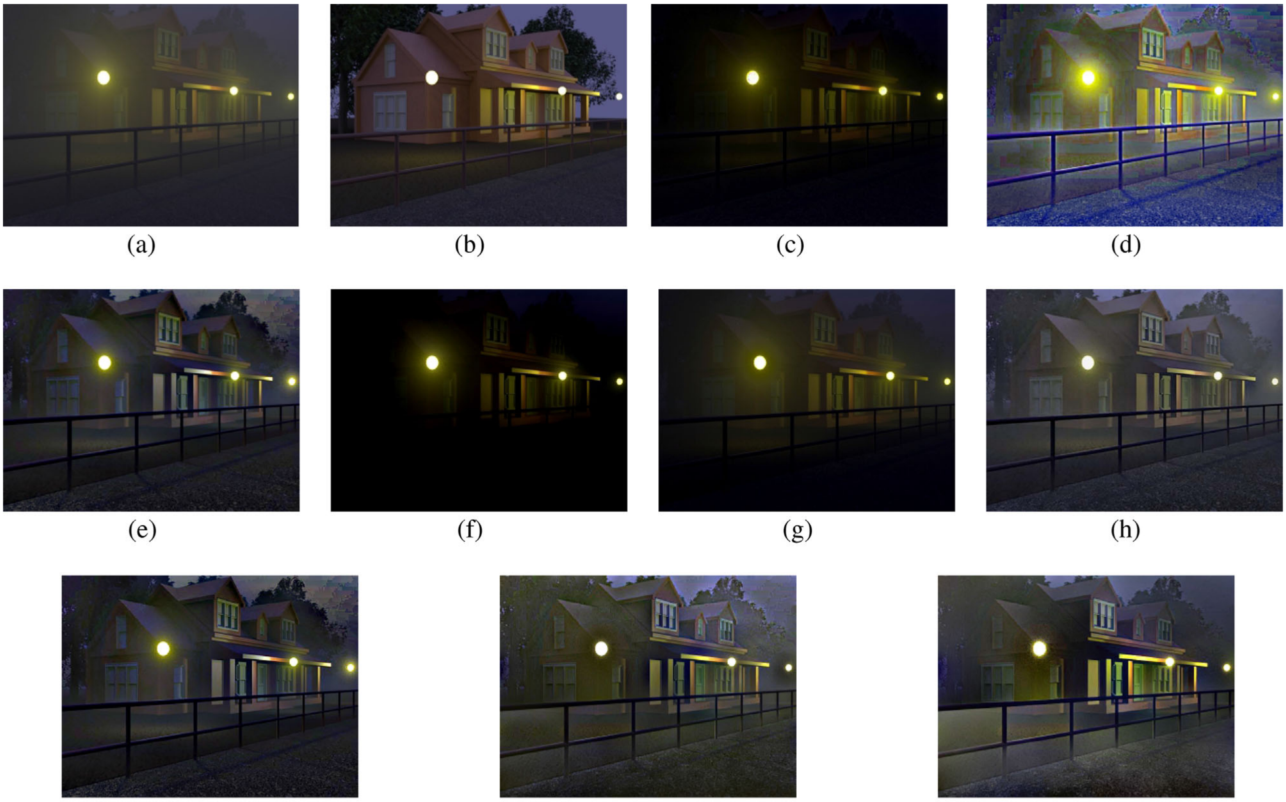

FIGURE 15 The results of image quality assessment.(a) Low-light hazy image. (b) Ground truth image. (c) DCP+HDRnet. (d) NIM. (e) MRP. (f) DehazeNet. (g) MSCNN. (h) HDF. (i) GDM. (j) PAB. (k) Ours

TABLE 3 The implementation times of the proposed and the comparative algorithms

Images	Size	DCP+HDRnet	NIM	MRP	DehazeNet	MSCNN	HDF	GDM	PAB	Ours
Figure 9	360*540	5.31	3.92	2.84	3.76	4.70	3.68	8.75	4.59	**5.72**
Figure 10	375*500	4.87	3.81	2.36	3.69	4.32	3.16	8.56	4.26	**4.98**
Figure 11	576*382	5.62	5.09	3.13	4.64	5.56	4.35	9.17	5.48	**5.91**
Figure 12	752*446	6.96	6.73	4.85	6.39	7.14	6.04	11.95	6.61	**7.24**
Figure 13	423*285	2.48	2.15	1.47	1.71	2.37	1.95	5.39	2.32	**2.56**
Figure 14	433*297	2.68	2.26	1.68	1.76	2.52	2.03	5.62	2.45	**2.84**

the implementation time is used to measure the algorithm. In order to compare with other methods, we use MATLAB to analyze the execution time of our experiment and collect some other real-time dehazing algorithms. The codes of DehazeNet, MSCNN, GDM, PAB are from their websites and the codes of DCP with HDRnet, NIM, MRP, HDF are provided in MATLAB. For a real-world low-light hazy image with size 360*540 (see in Figure 9), our proposed method spends more than 15s solving image depth model to obtain nonlinear coefficients. Specifically, each part (e.g., glow decomposition, light source segmentation, nonlinear image depth estimation, guided filter) consumes, respectively, 4.02, 0.92, 0.50, and 0.28 s. Table 3 shows all the runtimes of the proposed and other real-time dehazing algorithms from Figures 9 to 14. It is clear that our algorithm requires a little more processing time than other methods. This is because that the proposed method needs to solve nonlinear image depth estimation system.The part of glow decomposition consumes more time than other parts in our algorithm. It is concluded that the runtime of our algorithm meets the real-time requirement. Also, it is noteworthy that our algorithm is implemented with MATLAB and not optimized well, which could be accelerated by implementing with C++. Although our method needs more time, the results exhibit better on subjective and objective evaluation in most cases.

5 | DISCUSSION AND CONCLUSIONS

This paper mainly focuses on how to deal with the low-light image with haze, glow, and color shift produced by many kinds of light sources. For solving the color shift problem, we utilize the proposed color channel transformation to bring the image closer to reality. For segmenting the light source regions better, we put forward a new method by using gamma correction of channel difference with the threshold level to determine if the pixel belongs to light source regions. For the atmosphere light estimation, we estimate the ambient illuminance map with maximum reflectance prior and compute the atmosphere light in the light and non-light regions. The atmosphere light map is obtained by blending them together. For the transmission estimation, we create a nonlinear model among three image features (the luminance map, the saturation map, and the gradient map) of the depth map in the light areas and use the DCP in the non-light areas. Compared with others, our approach is more effective to remove haze, eliminate color distortion, improve the visibility, and reduce much more noise. Besides, our method looks more real in the image sky regions and has better edges preservation preformance. Unfortunately, our method still has some shortcomings that need to be researched further. First, there are some coefficients to be adjusted if necessary. Ideally, these parameters are supposed to be tuned self-adaptively. Second, a threshold value for the gamma correction of channel differences is obtained by training 500 low-light hazy images with light sources, which cannot be adaptively processed for different low-light scenes. In addition, the coefficients obtained by training the nonlinear model with samples are fixed values, so they cannot be adaptively processed for different low-light scenes. Finally, another issue is that the proposed method cannot satisfy the real-time dehazing task. Nevertheless, we will develop the self-adaptive and high computational effective algorithm to solve the problems in the future work.

ACKNOWLEDGEMENTS

This research is supported by National Natural Science Foundation of China under Grant No. 61705225.

CONFLICT OF INTEREST

No conflict of interest exits in the submission of this manuscript.

PERMISSION TO REPRODUCE MATERIALS FROM OTHER SOURCES

None.

DATA AVAILABILITY STATEMENT

Research data are not shared.

ORCID

Jianwei Lv https://orcid.org/0000-0002-6928-0720

REFERENCES

1. Narasimhan, S.G., Nayar, S.K.: Shedding light on the weather. In: 2003 IEEE Computer Society Conference on Computer Vision and Pattern Recognition. IEEE, Piscataway (2003)
2. Fattal, R.: Single image dehazing. ACM Trans. Graph. 27(3), 72 (2008)
3. Fattal, R.: Dehazing using color-lines. ACM Trans. Graph. 34(1), 13:1–13:14 (2014)
4. He, K., Sun, J., Tang, X.: Single image haze removal using dark channel prior. In: Proceedings of the IEEE Conference on Computer Vision and Pattern Recognition, pp. 1956–1963. IEEE, Piscataway (2009)
5. Ancuti, C., Ancuti, C., Hermans, C., Bekaert, P.: A fast semi-inverse approach to detect and remove the haze from a single image. In: Proceedings of the Asian Conference on Computer Vision, pp. 501–514. IEEE, Piscataway (2011)
6. Tan, R.T.: Visibility in bad weather from a single image. In: Proceedings of the IEEE Conference on Computer Vision and Pattern Recognition. IEEE, Piscataway (2008)
7. He, R., Huang, X.: Single image dehazing using non-local total generalized variation. In: Proceedings of the IEEE International Conference on Industrial Engineering and Applications, pp. 19–24. IEEE, Piscataway (2019)
8. Meng, G., Wang, Y., Duan, J., Xiang, S., Pan, C.: Efficient image dehazing with boundary constraint and contextual regularization. In: Proceedings of the IEEE International Conference on Computer Vision, Sydney, pp. 617–624. IEEE, Piscataway (2013)
9. Tang, K., Yang, J., Wang, J.: Investigating haze-relevant features in a learning framework for image dehazing. In: Proceedings of the IEEE Conference on Computer Vision and Pattern Recognition, pp. 2995–3002. IEEE, Piscataway (2014)
10. Zhu, Q., Mai, J., Shao, L.: A fast single image haze removal algorithm using color attenuation prior. IEEE Trans. Image Process. 24, 3522–3533 (2015)
11. Berman, D., Treibitz, T., Avidan, S.: Non-local image dehazing. In: Proceedings of the IEEE Conference on Computer Vision and Pattern Recognition, pp. 1674–1682. IEEE, Piscataway (2016)
12. Pei, S., Lee, T.: Nighttime haze removal using color transfer pre-processing and dark channel prior. In: Proceedings of the IEEE International Conference on Image Processing, pp. 957–960. IEEE, Piscataway (2012)
13. Zhang, J., Cao, Y., Wang, Z.: Nighttime haze removal based on a new imaging model. In: Proceedings of the IEEE International Conference on Image Processing, pp. 4557–4561. IEEE, Piscataway (2014)
14. Zhang, J., Cao, Y., Fang, S., Kang, Y., Chen, C.W.: Fast haze removal for nighttime image using maximumreflectance prior. In: Proceedings of the IEEE Conference on Computer Vision and Pattern Recognition, pp. 7418–7426. IEEE, Piscataway (2017)
15. Li, Y., Tan, R.T., Brown, M.S.: Nighttime haze removal with glow and multiple light colors. In: Proceedings of the IEEE International Conference on Computer Vision, pp. 226–234. IEEE, Piscataway 2015
16. Li, Y., Brown, M.S.: Single image layer separation using relative smoothness. In: Proceedings of IEEE Conference on Computer Vision and Pattern Recognition. IEEE, Piscataway (2014)
17. Yang, M., Liu, J., Li, Z.: Superpixel-based single nighttime image haze removal. IEEE Trans. Multimedia. 20(11), 3008–3018.20 (2018)
18. Yu, T., Song, K., Miao, P., Yang, G., Yang, H., Chen, C.: Nighttime single image dehazing via pixel-wise alpha blending. IEEE Access 7, 114619–114630 (2019)
19. Ancuti, C., Ancuti, C., De Vleeschouwer, C., Bovik, A.: Nighttime dehazing by fusion. In: Proceedings of the IEEE International Conference on Image Processing, pp. 2256–2260. IEEE, Piscataway (2016)
20. Ancuti, C., Ancuti, C., De Vleeschouwer, C.: D-HAZY: A dataset to evaluate quantitatively dehazing algorithms. In: Proceedings of IEEE International Conference on Image Processing, pp. 2226–2230. IEEE, Piscataway (2016)
21. Park, S., Yu, S., Moon, B., Ko, S., Paik, J.: Low-light image enhancement using variational optimization-based retinex model. IEEE Trans. Consum. Electron. 63, 178–184 (2017)
22. Guo, X., Li, Y., Ling, H.: LIME: Low-light image Enhancement via Illumination Map Estimation. IEEE Trans. Image Process. 26, 982–993 (2017)
23. Li, M., Liu, J., Yang, W., Sun, X., Guo, Z.: Structure-revealing Low-light image Enhancement via Robust Retinex Model. IEEE Trans. Image Process. 27, 2828–2841 (2018)
24. He, R., Guan, M., Wen, C.: SCENS: Simultaneous contrast enhancement and noise suppression for Low-light Images. IEEE Trans. Ind. Electron. in press (2020)
25. He, R., Guo, X., Shi, Z.: SIDE—A Unified framework for simultaneously dehazing and enhancement of nighttime hazy images. Sensors 20, 5300 (2020)

26. Lou, W., Li, Y., Yang, G., Chen, C., Yang, H., Yu, T.: Integrating haze density features for fast nighttime image dehazing. IEEE Access 8, 3318–3330 (2020)
27. Buchsbaum, G.: A spatial processor model for object color perception. J. Franklin Inst. 310(1), 1–26 (1980)
28. Land, E.: The retinex theory of color vision. Sci. Am. 237(6), 108–128 (1977)
29. He, K., Sun, J., Tang, X.: Guided image filtering. In: Proceedings of European Conference on Computer Vision. IEEE, Piscataway (2010)
30. Cai, B., Xu, X., Jia, K., Qing, C., Tao, D.: DehazeNet: An End-to-End System for Single Image Haze Removal. IEEE Trans. Image Process. 25, 5187–5198 (2016)
31. Ren, W., Liu, S., Zhang, H., Pan, J., Cao, X., Yang, M.: Single image dehazing via multi-scaleconvolutional neural networks. In: Proceedings of the European Conference on Computer Vision, pp. 154–169. IEEE, Piscataway (2016)
32. Kuanar, S., Rao, K.R., Mahapatra, D., Bilas, M.: Night time haze and glow removal using deep dilated convolutional network. arXiv:1902.00855v1 (2019). https://arxiv.org/abs/1902.00855v1
33. Wang, S.H., Zheng, J., Hu, H.M., Li, B.: Naturalness preserved enhancement algorithm for non-uniform illumination images. IEEE Trans. Image Process. 22(9), 3538–3548 (2013)
34. Klein, S., Pluim, J.P.W., Staring, M., Viergever, M.A.: Adaptive stochastic gradient descent optimization for image registration. Int. J. Comput. Vis. 81(3), 227–239 (2009)
35. Li, B., Peng, X., Wang, Z., Xu, J., Feng, D.: Aod-net: All-in-one dehazing network. In: Proceedings of the IEEE Conference on Computer Vision and Pattern Recognition, pp. 4770–4778, IEEE, Piscataway (2017)
36. Zhang, H., Patel, V.: Densely connected pyramid dehazing network. In: Proceedings of the IEEE Conference on Computer Vision and Pattern Recognition, pp. 3194–3203. IEEE, Piscataway (2018)
37. Gharbi, M., Chen, J., Barron, J.T.: Deep Bilateral Learning for Real-Time Image Enhancement. ACM Trans. Graph. 36(4), 118 (2017)
38. Hautiere, N., Tarel, J.P., Aubert, D., et al.: Blind contrast enhancement assessment by gradient ratioing at visible edges. Image Anal. Stereol. 27(2), 87–95 (2011)
39. Yu, X., Xiao, C., Deng, M., et al.: A classification algorithm to distinguish image as haze or non-haze. In: 2011 Sixth International Conference on Image and Graphics (ICIG). IEEE, Piscataway (2011)
40. Mittal, A., Moorthy, A.K., Bovik, A.C.: No-Reference image quality assessment in the spatial domain. IEEE Trans. Image Process. 21(12), 4695–4708 (2012)
41. Wang, Z., et al.: Image quality assessment: From error visibility to structural similarity. IEEE Trans. Image Process. 13(4), 600–612 (2004)
42. Economopoulos, T.L., Asvestas, P.A., Matsopoulos, G.K.: Contrast enhancement of images using partitioned iterated function systems. Image Vis. Comput. 28(1), 45–54 (2010)
43. Johnson, D.J., Rahman, Z.U., Woodell, G.A., et al.: A comparison of visual statistics for the image enhancement of FORESITE aerial images with those of major image classes. Proc. SPIE - Int. Soc. Opt. Eng. 6246, 624601–624601-8 (2006)
44. Liao, Y., Su, Z., Liang, X., Qiu, B.: Hdp-net: Haze density prediction network for nighttime dehazing. In: Proceedings of the Pacific Rim Conference on Multimedia, pp. 469–480. Springer, New York (2018)

How to cite this article: Lv, J., Qian, F., Zhang, B.: Low-light image haze removal with light segmentation and nonlinear image depth estimation. IET Image Process. 16, 2623–2637 (2022). https://doi.org/10.1049/ipr2.12513